

SUPPORTING MATERIAL

ARROW layer sequence

layer	1	2	1	2	1	2	core	2	1	2	1	2	1
thickness	1,876	100	268	100	268	100	5,000	132	286	146	300	128	3,016

Table S1: Thickness of the ARROW layers in nm. Composition: 1 = SiO₂, 2 = SiN. The silicon substrate is below the first layer and the last layer is followed by air.

Trap analysis with 200 nm particles

The 1 μm particles described in the main text could be confined very tightly. To explore the complete topology of the trap an appreciable probability of particle excursions beyond the central region is required. For this we chose 200nm particles which could be trapped intermittently and still be tracked with a long working distance imaging system. Strong fluctuations in the fluorescence signal (Fig. S1a) are evidence that the particle undertakes excursions over a wide range of the excitation/detection volume. The reduced particle size requires higher feedback voltages due to a reduced mobility of $\mu_e \approx 6 \cdot 10^{-3} \mu\text{m/s}\cdot\text{m/V}$ and a higher diffusion speed $v_r \approx 4 \cdot \Delta z \cdot D$ ($D \approx 2.5 \mu\text{m}^2/\text{s}$, $2\Delta z$: trapping region), which taken together scale approximately as $U_{\text{max}} \sim 1/r^3$. For similar trapping performance, modulation rate and mean count rate must be scaled as $\Omega_{\text{mod/sig}} \sim 1/r$ to avoid processing lag or bandwidth limitations. These requirements are easily met. Observed particle residence times in the trap were typically on the order of 10-20sec. This is mainly due to the poor confinement in x and y, even at elevated guiding beam powers of 33mW (at the

particle location). The gradient force scales in the Rayleigh regime with the polarizability of the particle, which in turn is proportional to the particle volume. As shown in Fig. 4d of the main text the particle tends to evenly sample the complete x extension of the channel. Nevertheless, the trap is capable of confining the particle in z to less than $\pm 0.5\mu\text{m}$ corresponding to an effective spring constant of $k_z \approx 16\text{nN/m}$.

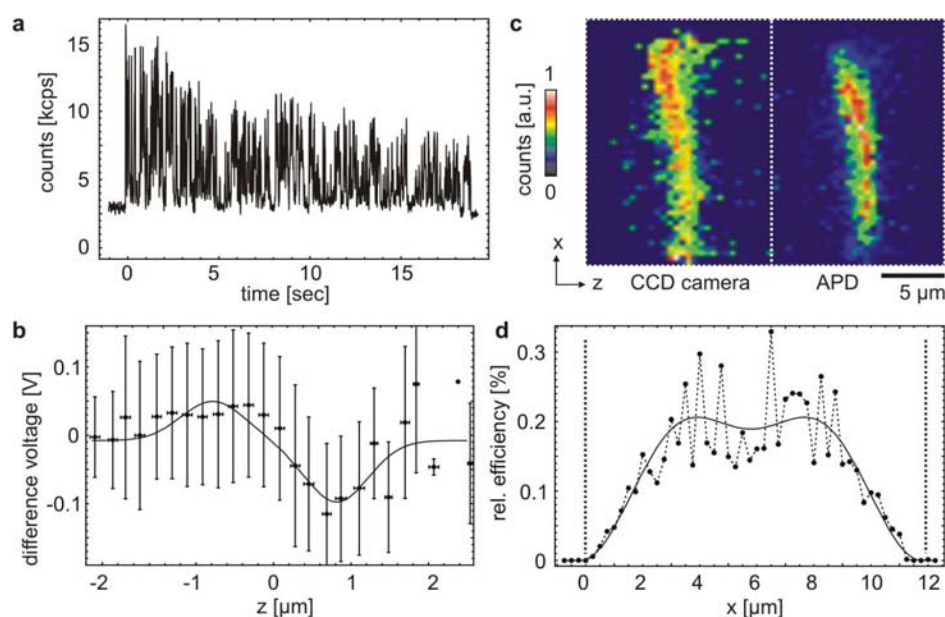


Fig. S1: Capture of a 200nm latex bead in the electro-optical trap.

a: Fluctuating fluorescence signal of a single bead. **b:** Demodulated position signal used for feedback actuation. **c:** Maps of the fluorescence count rates for the CCD and APD detectors as a function of particle position as obtained from the CCD image. **d:** Relative detection efficiency for the APD detector over the cross-section of the waveguide. The vertical dotted lines indicate the channel walls.

Fig. S1b shows the restoring voltage plotted against the particle z position. Despite the noise that is caused by the fair SNR for these small particles a dispersive curve can clearly be distinguished in the mean response, the shape of which resembles the expected difference of two Gaussians offset by $1.9\mu\text{m}$.

The excursions in x allow us to investigate the detectivity function of the waveguide by comparing the fluorescence signal intensities s_{APD} and s_{CCD} measured by the APD and the CCD sensor for different particle locations. Under the assumption that the collection efficiency for the CCD sensor is uniform across the waveguide, the CCD signal is a measure of the excitation rate at any location in the field of view. The detectivity is therefore proportional to the ratio $\eta_{\text{rel}} = s_{\text{APD}}/s_{\text{CCD}}$. We show the time averaged signal for a single particle received by the CCD and the APD in Fig. S2c (APD count rate $\approx 3\text{kcps}$) as a function of the particle position that was simultaneously obtained from the CCD images. It can be seen that the APD signal gradually drops when the particle approaches the waveguide walls at the top and bottom of the fluorescence map, while the CCD signal remains as bright as in the center of the waveguide. The resulting detectivity is plotted in Fig. S1d and fitted with the first two transverse modes that exist in the waveguide. The relative weight amounted to 68% for the fundamental and 32% for the first order mode. This is surprising, since the narrow solid core sections ($4\mu\text{m}$ ridge width) beyond the taper region are expected to favor the fundamental and suppress any higher modes. It appears that non-uniformities and roughness in the waveguide structures lead to cross-power leakage of the first into the fundamental mode of the liquid core.

From the distribution of the detectivity we can predict that stable trapping would be achieved if the particle is kept at least $2\mu\text{m}$ from the waveguide boundaries. We also

remark that the approximation of the detectivity function by a Gaussian typically applied in fluorescence correlation analysis may pose a source of inaccuracy.

MOVIE DESCRIPTIONS

Supplementary Movie S1: Capture of a 1 μm fluorescent latex bead in the electro-optical trap

The trapping region at the asymmetric intersection of a liquid-core waveguide and two solid-core waveguides is shown in bright field illumination. After a few seconds a microbead enters the trap as a dark dot from the right and starts to emit strong fluorescence under the excitation from the solid core waveguides. The excitation light and the guiding beam along the liquid core are blocked with filters. Later, the illumination is turned off to avoid background interference in the fluorescence detection.

file name: Movie 1r.avi (avi-format, 292kb)

Supplementary Movie S2: Single particle trapping in presence of multiple microbeads

This movie illustrates the fact that the active optofluidic traps is a true single particle trap. We show two 1 μm fluorescent beads, one of which (left) is caught in the trap. The other bead (right) is subject to diffusion, drift and corrective electrokinetic forces induced by the trapped bead. It is not drawn into the trapping region.

file name: Movie 2r.avi (avi-format, 467kb)

Supplementary Movie S3: Fluorescence from DNA of a trapped E.-coli bacterium

A fluorescently labeled E.-coli bacterium is captured in the electro-optical trap and suspended until photobleaching reduces the fluorescence signal far below the

background. The slightly elongated shape of the bacteria allows for observation of the free rotational motion around its fluorescence center of mass. The bright spots at the solid to liquid-core waveguide intersections represent background luminescence of the SiN ARROW layers.

file name: Movie 3r.avi (avi-format, 198kb)